IEEE Access
Multidisciplinary ⋮ Rapid Review ⋮ Open Access Journal

Received 27 February 2024, accepted 14 March 2024, date of publication 18 March 2024, date of current version 27 March 2024.

Digital Object Identifier 10.1109/ACCESS.2024.3378744

RESEARCH ARTICLE

Passive Voltage Amplification in FE-FE-DE Heterostructure

BHASKAR AWADHIYA[1], SAMEER YADAV[2], YASHWANTH NANJAPPA[1], (Senior Member, IEEE), ABHISHEK PAHUJA[2], SHIVENDRA YADAV[3], AND SACHIN AGRAWAL[4]

[1]Department of Electronics and Communication Engineering, Manipal Institute of Technology, Manipal Academy of Higher Education, Manipal, Udupi, Karnataka 576104, India
[2]Department of Electronics and Communication, Koneru Lakshmaiah Education Foundation, Vaddeswaram, Guntur, Andhra Pradesh 522302, India
[3]Department of Electronics and Communication Engineering, Sardar Vallabhbhai National Institute of Technology, Surat, Gujarat 395007, India
[4]Department of Electronics and Communication Engineering, National Institute of Technology Delhi, Delhi 110036, India

Corresponding author: Yashwanth Nanjappa (yashwanth.n@manipal.edu)

This work was supported by the Manipal Academy of Higher Education, Manipal.

ABSTRACT In this article, we have studied passive voltage amplification in FE-FE-DE heterostructure. We have stacked two different ferroelectric oxides; one is second-order transition ferroelectric material (continuous transition ferroelectric material) and the other is first-order transition ferroelectric material (discontinuous transition ferroelectric material). Both ferroelectric materials have different polarities of anisotropy constant (β), which is tuned by varying the ferroelectric thickness and thus leads to its cancellation. The nullification of the anisotropy constant will reduce the non-linearity of the ferroelectric oxide and provide efficient matching between the ferroelectric and dielectric capacitance, which in turn delivers the higher voltage amplification in the heterostructure. Also, dynamic response and temperature analysis of heterostructure are studied further. It is observed that dielectric when added in series with the isolated ferroelectric capacitor the curie temperature shifts to a lower value.

INDEX TERMS Ferroelectric (FE), dielectric (DE), heterostructure, passive voltage amplification.

I. INTRODUCTION

Ferroelectric materials [1], [2], [3] are well known for the attributes of spontaneous polarization [4], they can be polarized when there is no electric field. Polarization direction can be reoriented when it is exposed to an electric field. This is in contrast with the dielectric material, where the applied electric field and polarization charge constitute a straight alliance. Ferroelectricity was discovered experimentally a hundred years ago [5] and Rochelle salt ($NaKC_4H_4O_4{\cdot}4H_2O$) and Potassium dihydrophosphate (KH_2PO_4) were a few materials on which experiments were performed. These materials had the disadvantage of being fragile and water soluble. Out of numerous functional materials, traditional perovskite oxides have a broad spectrum of application capabilities that are significantly related to common domestic applications. The commercial usage of perovskites is covered but not limited to many areas such as microelectronics, memories, sensors, storage systems, energy harvesting, mechanical processing, piezoelectric actuators, ultrasonic energy converters, optical and numerous other related devices [6]. The search for robust ferroelectric material concluded with the recognition of perovskite materials specially first and second order transition materials [7], [8], [9]. These materials have a general formula of ABO_3, here A symbolizes di/monovalent atom, B symbolizes tri/tetravalent atom and O symbolizes oxygen atom. Also, they have tetragonal crystal lattice structure, therefore one side of unit cell is prolonged as compared to the other two sides and angle between three of them is 90^0. This non centro-symmetricity in the lattice assembly of perovskite remains the prime cause behind the traits of ferroelectricity and thus ensures spontaneous dipole moment and the electric polarization. The basic understanding of physics in ferroelectrics is well understood by phenomenological model based on Landau-Ginzburg-Devonshire theory generally called as Landau theory of phase transitions [10]. This model is useful in the study of negative capacitance existence in ferroelectric materials. According to this theory, a ferroelectric material can have a negative capacitance, which manifests as a double-well shaped in the ferroelectric's

The associate editor coordinating the review of this manuscript and approving it for publication was Shuo Sun.

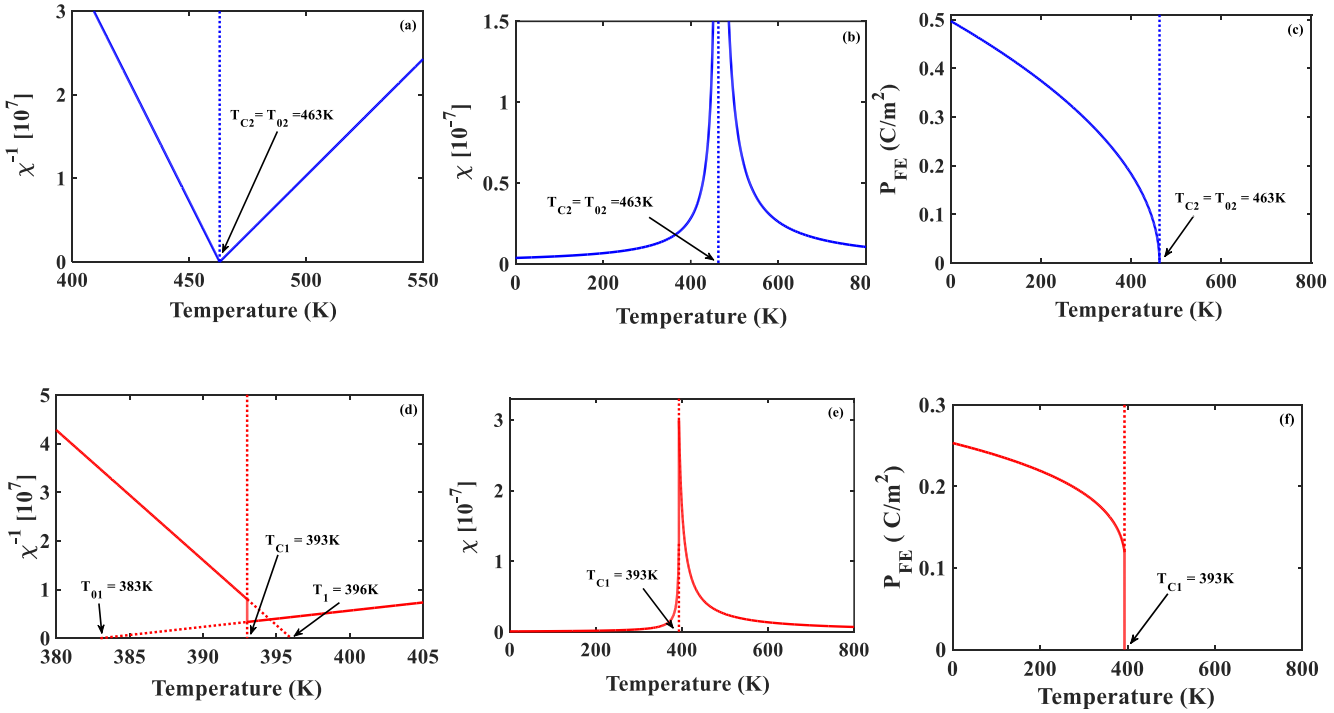

FIGURE 1. (a) Susceptibility (b) Inverse susceptibility (c) Spontaneous polarization of *PZT* vs. temperature (d) Susceptibility (e) Inverse susceptibility (f) Spontaneous polarization of $BaTiO_3$ vs. temperature.

free energy when an electric field is applied. Despite being predicted more than 70 years ago, initially most scientists thought it was impossible to detect negative capacitance in an experiment while later some work reported its existence [11], [12], [13], [14], [15]. But it's crucial to pay attention to the negative capacitance signature. This is due to the fact that, it has the ability to magnify an applied voltage, which might be used to lower the power dissipation in post-CMOS era [16]. Many reported works have shown the potential of negative capacitance in ferroelectric in steep switching devices [17], [18], circuits [19], [20], memory [21], [22] etc. In this work we have tried to utilize negative capacitance in two differently ordered perovskite materials to enhance amplification and reduce the non-linearity. The mathematical equations are solved in MATLAB with anisotropy constants of ferroelectric material, for obtaining the results. The breakdown of how the paper is organized: Section II covers the categorization and fundamental formula for choosing ferroelectric materials for voltage amplification. Section III discusses the impacts that resulted from the FE-FE structure. Sections IV and V, respectively, investigate FE-FE-DE heterostructure static and dynamic response. In section V, the effects of temperature on FE-FE-DE heterostructure are examined, and section VI concludes the study done in the article.

II. SECOND ORDER TRANSITION AND FIRST ORDER TRANSITION FERROELECTRIC MATERIAL

Perovskite materials can be sub-classified based on the transition between ferroelectric to paraelectric phase [23]. Materials that possess a continuous transition between the ferroelectric and paraelectric phases are termed second-order transition material and those which possess a discontinuous phase transition between ferroelectric and paraelectric phase are coined as first-order transition material. Here, we have Lead Zirconium Titanate ($PbZr_{1-x}Ti_xO_3$) [24], [25] and Barium titanate ($BaTiO_3$) [26] as second and first order transition material respectively. In second order transition material Curie-Weiss temperature (T_{02}) coincide with Curie temperature (T_{C2}). Transition between ferroelectric to paraelectric phase for second order transition can be understood in terms of electric susceptibility which are expressed in equation (1) and (2):

$$\chi_F^{-1} = 2\alpha_{02}\,(T_{02} - T)\,;\ T < T_0 \tag{1}$$

$$\mathrm{z}\chi_P^{-1} = \alpha_{02}\,(T - T_{02})\,;\ T > T_0 \tag{2}$$

where χ_F and χ_P represents electrical susceptibility in the ferroelectric and paraelectric phase. α_{02} represents positive material dependent constant for PZT. Fig. 1(a) shows the $\chi - T$ forPZT. Continuous transition is observed in this characteristic as Curie-Weiss temperature (T_{02}) is equal to Curie temperature(T_{C2}) also electric susceptibility becomes infinite at Curie temperature. Fig. 1(b) shows the $\chi^{-1} - T$ and for PZT, here it can be observed that gradient of inverse permittivity in the ferroelectric phase is twice that of the paraelectric phase. Further, Fig. 1(c) shown the spontaneous polarization (P_{FE}) in the ($PbZr_{1-x}Ti_xO_3$) versus temperature which is obtained by solving equation (3). The phase transition eventuates at $T_{C2} = T_{02}$ and the spontaneous

polarization falls to zero.

$$P_{FE} = \sqrt{\frac{\alpha_{02}\,(T_{02} - T)}{\beta_2}} \tag{3}$$

In first order transition material Curie-Weiss temperature doesn't coincide with Curie temperature. The Curie-Weiss temperature (T_{01}) is smaller than Curie temperature (T_{C1}) which is responsible for discontinuous transition between ferroelectric and paraelectric phase. Transition between ferroelectric to paraelectric phase can be explained in terms of electric susceptibility of second order transition material are expressed in equation (5) and (6):

$$\chi_F^{-1} = 8\alpha_{01}\,(T_1 - T)\,;\ T < T_C \tag{4}$$

$$\chi_P^{-1} = \alpha_{01}\,(T - T_{01})\,;\ T > T_C \tag{5}$$

α_{01} represents positive material dependent constant for $BaTiO_3$ Fig. 1(d) shows the $\chi - T$ characteristics for $BaTiO_3$. Discontinuous transition between ferroelectric and paraelectric phase is observed, as in these characteristics as Curie-Weiss temperature (T_{01}) does not coincides with the Curie temperature(T_{C1}). It is clear from the shown figure that electric susceptibility has a finite value at Curie temperature. The relationship between T_{C1} and T_{01} can be established as: $T_{C1} = T_{01} + 3\beta_1^2/16\alpha_{01}\gamma_1$. As per the equation Curie-Weiss temperature (T_{01}) is smaller than Curie temperature(T_{C1}). Fig 1(e) shows the $\chi^{-1} - T$ characteristics for $BaTiO_3$. The gradient of inverse permittivity in ferroelectric phase is approximately eight times that of paraelectric phase. The Curie–Weiss temperature (T_{01}) is obtained by extrapolating the temperature in the paraelectric phase, and the temperature (T_1) is obtained by extrapolating the temperature in the ferroelectric phase. The relationship between T_1 and T_0 can be established as: $T_1 = T_{01} + \beta_1^2/4\alpha_{01}\gamma_1$. Further Fig. 1(f) shown the spontaneous polarization (P_{FE}) in the Barium Titanate ($BaTiO_3$) versus the temperature which is obtained by solving equation (6).

$$P_{FE}^2 = \frac{-\beta_1}{2\gamma_1} + \frac{\sqrt{\beta_1^2 - 4\alpha_{01}(T - T_{01})\gamma_1}}{2\gamma_1} \tag{6}$$

The phase transition occurs at T_{C2} and the discontinuity of the spontaneous polarization appears at T_{C2}. Further second-order and first order transition material can also be differentiated based on value anisotropy constants(α, βandγ) of ferroelectric material. Second order transition materials have positive value of β_2 and γ_2 and negative value of α_2, while first order transition materials have positive value of γ_1 and negative value of α_1 andβ_1. It is worth noting that these constants are thickness dependent. This property of first and second order transition material is utilized in the heterostructure [11], [27], [28], [29], [30], [31] to reduce the nonlinearity and achieve the efficient voltage amplification which has been discussed in the further section of the article.

III. FERROELECTRIC CAPACITOR

Ferroelectrics manifests negative capacitance [32], [33], [34], [35], [36], [37], [38], [39], [40], [41], [42], [43], [44] and the dynamics of ferroelectric material can be understood by Landau-Khalatnikov equation [45], [46], which says the rate change of polarization charge can be expressed as shown in equation (7).

$$\rho\frac{dQ_{FE}}{dt} = -\frac{dU_{FE}}{dQ_F} \tag{7}$$

where ρ represents the ferroelectric damping constant, Q_F is the polarization charge ($Q_F = P \times A$, here P represents remanent polarization and $A(45nm \times 1\mu m)$ is the area of heterostructure) and U being the net energy of the ferroelectrics that could be expressed as shown in equation (8).

$$U_{FE} = \frac{\alpha}{2}{Q_{FE}}^2 + \frac{\beta}{4}{Q_{FE}}^4 + \frac{\gamma}{6}{Q_{FE}}^6 - Q_{FE}V_{FE} \tag{8}$$

where α, β and γ represents anisotropy constants of ferroelectric oxide, solving the above equations results in equation (9).

$$V_{FE} = \alpha Q_{FE} + \beta {Q_{FE}}^3 + \gamma {Q_{FE}}^5 + \rho\frac{dQ_{FE}}{dt} \tag{9}$$

under steady state condition the above equation reduces to the equation (10).

$$V_{FE} = \alpha Q_{FE} + \beta {Q_{FE}}^3 + \gamma {Q_{FE}}^5 \tag{10}$$

since we are using stacked ferroelectric oxide in this heterostructure, the voltage dropped across both the ferroelectric oxide can be constituted as arithmetic sum of individual voltage drop i.e., $V_{FE} = V_{FE1} + V_{FE2}$

$$V_{FE} = (\alpha_1 + \alpha_2)Q_{FE} + (\beta_1 + \beta_2){Q_{FE}}^3 + (\gamma_1 + \gamma_2){Q_{FE}}^5 \tag{11}$$

where α_1, β_1 and γ_1 represents anisotropy constants of Barium Titanate ($BaTiO_3$) and α_2, β_2 and γ_2 represents anisotropy constants of Lead Zirconium Titanate ($PbZr_{1-x}Ti_xO_3$). Here x reperesents the content of content of titanium in lead zirconium titanate. x here is taken as 0. Similar, to the voltage, the net energy of both the ferroelectric oxide can represented as arithmetic sum of individual energy i.e., $U_{FE} = U_{FE1} + U_{FE2}$

$$U_{FE} = \left(\frac{\alpha_1 + \alpha_2}{2}\right){Q_{FE}}^2 + \left(\frac{\beta_1 + \beta_2}{4}\right){Q_{FE}}^4 + \left(\frac{\gamma_1 + \gamma_2}{6}\right){Q_{FE}}^6 \tag{12}$$

anisotropy constant for Lead Zirconium Titanate (PZT) and Barium Titanate ($BaTiO_3$) [47] has been tabulated in Table 1. As mentioned in the earlier section, the anisotropy constant has opposite polarity for both materials, further the ferroelectric thickness for both, is tuned in an efficient manner which leads to the cancellation of $\beta_1 + \beta_2$. It is important to note this cancellation can be achieved only if the first and second order

TABLE 1. Simulation parameter for the ferroelectric oxides ([1] $BaTiO_3$ and [2] PZT).

$Parameters$	$BaTiO_3$	PZT
$\alpha_{1,2}\ (cm/F)$	-1×10^{10}	-4.50×10^{9}
$\beta_{1,2}(cm^5/F\ Coul^2)$	-8.90×10^{18}	5.20×10^{18}
$\gamma_{1,2}(cm^9/F\ Coul^4)$	4.50×10^{28}	3.75×10^{27}
$t_{FE\ 1,2}(nm)$	120	108

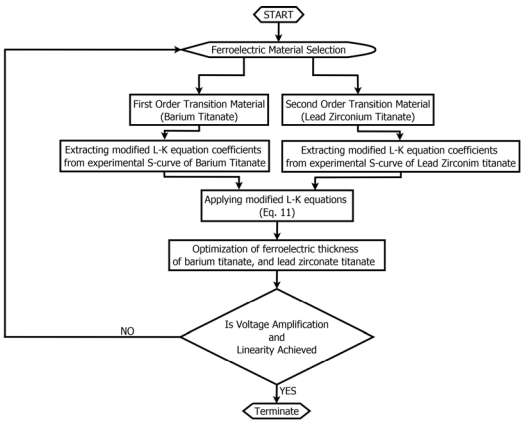

FIGURE 2. Explanation of ferroelectric thickness optimization.

ferroelectric oxides are connected in series. It won't be possible to achieve the same if two first order or two second order FE oxides are connected in series. Fig 2 shows the detailed explanation of ferroelectric thickness optimization. Fig. 3(a) depicts the schematic diagram of an isolated ferroelectric capacitor attached to a voltage source. Fig 3(b) depicts the charge as a function of voltage for a ferroelectric capacitor, an increase in voltage across ferroelectric guides a decrease in ferroelectric charge, which validates negative capacitance in ferroelectrics. For $t_{FE2}=0$ the coercive voltage is smaller while for $t_{FE1}=0$ the coercive voltage is higher. However, when $t_{FE2}=108nm$ and $t_{FE1}=120nm$, the coercive voltage is higher as compared to both the cases. Fig. 3(c) depicts energy landscape of a ferroelectric capacitor. For all three cases, the inverted parabola can be visualized which once again confirms the existence of negative capacitance. The negative capacitance state is volatile in nature, which can be understood by the energy landscape of ferroelectric, as a small perturbation while placing a charge on the top of an inverted parabola, may result in its fall to one of the minima. Hence a negative capacitance condition in ferroelectric capacitor is highly unstable and can observed only in time-dependent switching experiments. For stabilizing the NC state, a small dielectric capacitance should be added in series to an isolated ferroelectric capacitor which is discussed in the next section.

IV. FE-DE HETEROSTRUCTURE

Fig. 4(a) depicts the schematic diagram of an FE-FE-DE heterostructure connected to a voltage source. The thickness of dielectric oxide (t_{DE}) is taken as $10nm$ and its dielectric constant (ε_r) is 4. The unstable negative capacitance state in isolated ferroelectric state can be stabilized by the addition of series dielectric capacitor, provided that the ferroelectric capacitance should be greater than the dielectric capacitance. Also, it is quite interesting to notice that, if ferroelectric capacitance is very close to dielectric capacitance, high amplification is observed in the heterostructure. Ferroelectric capacitance for the isolated ferroelectric capacitor can be obtained by differentiating equation (11).

$$C_{FE}=\frac{1}{(\alpha_1+\alpha_2)+(\beta_1+\beta_2){Q_{FE}}^2+(\gamma_1+\gamma_2){Q_{FE}}^4} \tag{13}$$

The capacitance for dielectric capacitor can be expressed as follows:

$$C_{DE}=\frac{\varepsilon_o\varepsilon_r A}{t_{DE}} \tag{14}$$

here ε_o represents the absolute permittivity. Fig.4 (b) shows the capacitance versus charge characteristics of the heterostructure. The ferroelectric capacitance is greater than dielectric capacitance in all three cases. However, when $t_{FE2}=108nm$ and $t_{FE1}=120nm$ the ferroelectric capacitance is closely matched to dielectric capacitance. Close matching of both capacitances is the essential criteria for voltage amplification. Hence for this thickness combination voltage amplification will be highest which will be discussed later. Also, in the heterostructure we are having series combination of capacitor, so the charge in ferroelectric will be same as that of dielectric ($Q_{FE}=Q_{DE}$). Applying Kirchhoff's voltage law in the heterostructure, we can write $V_S=V_{FE}+V_{DE}$.

$$V_S=(\alpha_1+\alpha_2)Q_{FE}+(\beta_1+\beta_2){Q_{FE}}^3+(\gamma_1+\gamma_2){Q_{FE}}^5+\frac{Q_{FE}}{C_{DE}} \tag{15}$$

Fig.4 (c) shows the charge versus voltage characteristics of heterostructure which can be obtained by solving equation (15). This characteristic doesn't show any signature of negative slope and makes sure that it has a positive capacitance and is stable in nature. Similarly, the total energy can be heterostructure is sum individual energy of ferroelectric and dielectric capacitance $U_T=U_{FE}+U_{DE}$.

$$U_T=\left(\frac{\alpha_1+\alpha_2}{2}\right)Q_{FE}^2+\left(\frac{\beta_1+\beta_2}{4}\right)Q_{FE}^4+\left(\frac{\gamma_1+\gamma_2}{6}\right)\times Q_{FE}^6+\frac{Q_{FE}^2}{2C_{DE}} \tag{16}$$

Fig.4 (d) shows the energy landscape of heterostructure which can be obtained by solving equation (16). It is quite interesting to see that total energy of the system is stabilized and dual well in the energy landscape will advent adjacent to each other and becomes flatter. This flatness in the energy

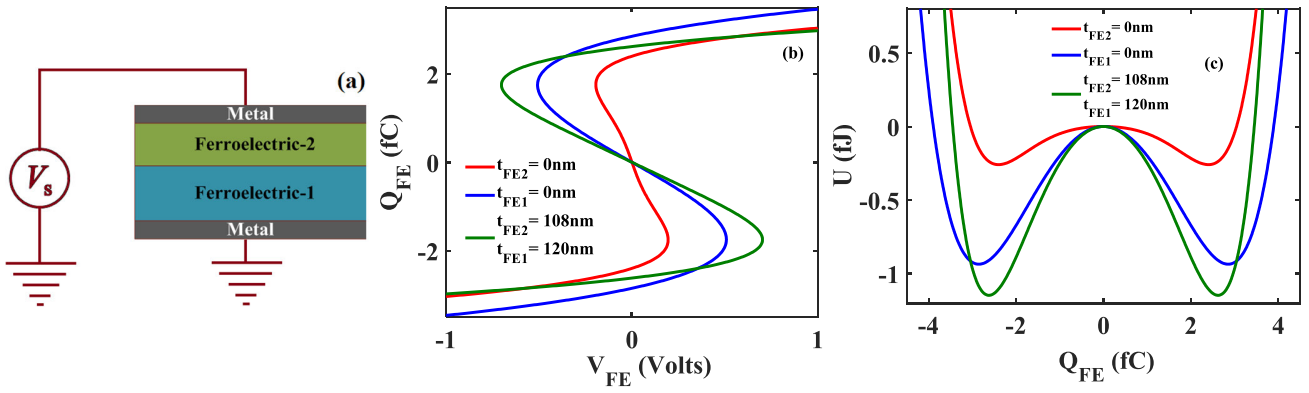

FIGURE 3. (a) Schematic of isolated heterostructure connected to voltage source (b) $Q_{FE} - V_{FE}$ characteristics (c) Energy landscape for an isolated ferroelectric capacitor.

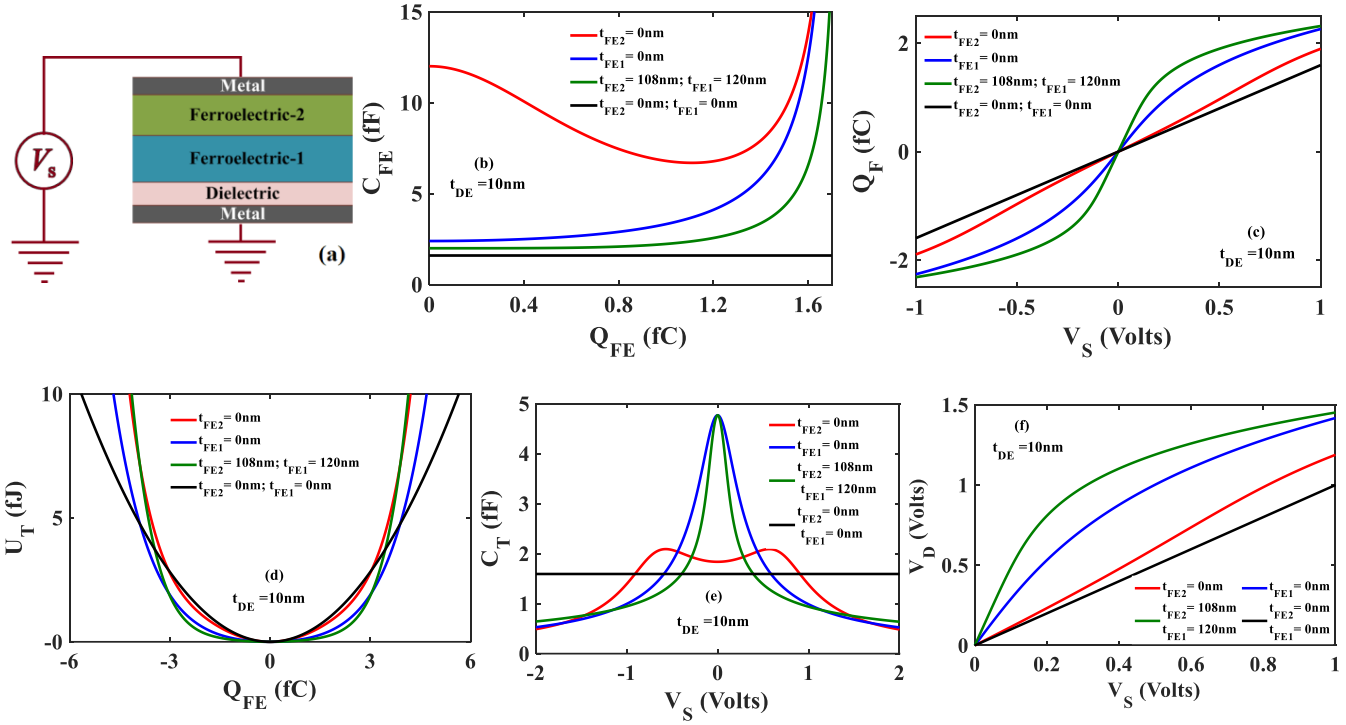

FIGURE 4. (a) Schematic of FE-FE-DE heterostructure connected to voltage source (b)$C_{FE} - Q_{FE}$ (c) $Q_{FE} - V_S$ (d) Energy landscape (e) Capacitance (f) Voltage amplification characteristics of FE-FE-DE heterostructure.

landscape is higher for $t_{FE2} = 108nm$ and $t_{FE1} = 120nm$ as compared to $t_{FE2} = 0$ and $t_{FE1} = 0$. This gets further confirmed from capacitance versus voltage characteristics shown in Fig. 4 (e). In the heterostructure, both the capacitances are in series to each other, hence the total capacitance of the heterostructure is given as shown in equation (17).

$$C_T = \frac{C_{FE}C_{DE}}{C_{FE} + C_{DE}} \tag{17}$$

where $C_{FE} = C_{FE1}||C_{FE2}$. The increment in the total capacitance is a violation of principles of circuit theory and electrostatics. As equivalent capacitance of two capacitance in series combination is always lower than both of them. This contravention of the classical law has only one explanation which is existence of negative capacitance. The co-relation between supply voltage and voltage across dielectric capacitor can be represented as shown in equation (18).

$$V_D = V_S \times \frac{|C_{FE}|}{|C_{FE}| - C_{DE}} \tag{18}$$

The above equation shows that voltage drop across dielectric (V_D) can be higher than the supply voltage (V_S), provided $|C_{FE}| > C_{DE}$. Also, when C_{FE} is in the proximity with the C_{DE} i.e. ($|C_{FE}| \sim C_{DE}$) the voltage amplification is highest. Fig. 4(f) shows the voltage drop across dielectric versus supply voltage characteristics. For $t_{FE2} = 108nm$

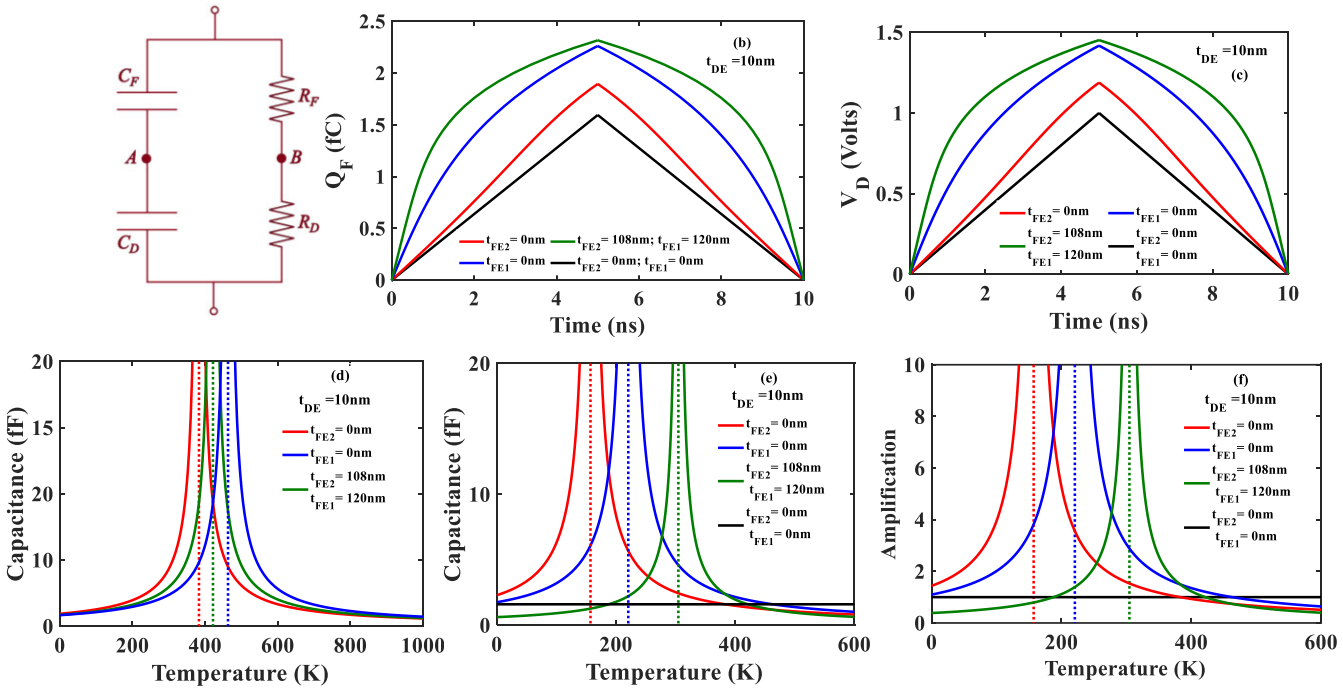

FIGURE 5. (a) Circuit configuration for heterostructure (b) Charge as a function of time (c) Voltage drop across dielectric as a function of time (d) Capacitance versus temperature characteristics of isolated ferroelectric capacitor (e) Capacitance versus temperature of heterostructure (f) Amplification versus temperature characteristics of heterostructure.

and $t_{FE1} = 120nm$ the voltage amplification is highest as compared to other two cases. It is interesting, that amplification will be present till $C_{AB} < |C_{FE}| - C_{DE}$ even if interface charge exists. Also, for obtaining the amplification for every voltage value nonlinearity should be suppressed completely.

V. DYNAMIC RESPONSE OF THE HETEROSTRUCTURE

In this section, we have discussed the dynamic response FE-FE-DE heterostructure. Circuit equivalent for the heterostructure is shown in Fig. 5(a). The ideal capacitor is the one in which infinite resistance is in parallel to it, however in the equivalent circuit for heterostructure, we have considered a practical scenario and resistances R_{FE} and R_{DE} can be seen parallel to the corresponding capacitors. Here it is interesting to note that the potential spotted at node A is unaltered by the existence of resistance and completely reliant on the capacitors. Therefore, this heterostructure is considered as a nonleaky FE-FE-DE heterostructure [48]. Earlier because of steady state analysis we had ignored $\rho dQ_{FE}/dt$ term of equation (9). Now, as we are doing the dynamic analysis this term can't be ignored and the modified equation (19) is mentioned below:

$$V_S = \alpha Q_{FE} + \beta {Q_{FE}}^3 + \gamma {Q_{FE}}^5 + \rho \frac{dQ_{FE}}{dt} + \frac{Q_{FE}}{C_{DE}} \quad (19)$$

Fig. 5(b) shows variation in the charge with respect to time when triangular pulse of $1V$ magnitude ($0V \rightarrow 1V \rightarrow 0V$) and frequency of 0.1 GHz is employed at the input (V_S) of heterostructure. Replacing $Q_{FE} = Q_{DE} = V_{DE}C_{DE}$ in equation (19), result in the following:

$$V_S = \alpha V_{DE}C_{DE} + \beta V_{DE}{C_{DE}}^3 + \gamma V_{DE}{C_{DE}}^5 + \rho \frac{dV_{DE}C_{DE}}{dt} + \frac{V_{DE}C_{DE}}{C_{DE}} \quad (20)$$

The voltage drop across the dielectric capacitor as a function of time is shown in Fig. 5(c) which is obtained by solving equation (14). For $t_{FE2} = 108nm$ and $t_{FE1} = 120nm$ the voltage amplification with respect to time is highest as compared to other two cases.

VI. TEMPERATURE ANALYSIS OF THE HETEROSTRUCTURE

In this section, we have studied the temperature analysis of the heterostructure [49]. Prior to that we have done the temperature analysis of the isolated ferroelectric capacitor. The capacitance of the isolated ferroelectric capacitor can be approximated at less value of charge, is mentioned in equation (21). (Also γ is temperature independent anisotropy constant hence can be neglected)

$$C_{FE} \approx \frac{1}{(\alpha_1 + \alpha_2)} \quad (21)$$

where $\alpha_1$and α_2 are temperature dependent anisotropy constant for $BaTiO_3$ andPZT respectively. $\alpha_1 = \alpha_{01}(T - T_{01})$

and $\alpha_2 = \alpha_{02}\,(T - T_{02})$

$$C_{FE} \approx \frac{1}{T\,(\alpha_{01}+\alpha_{02}) - \alpha_{01}T_{01} - \alpha_{02}T_{02}} \tag{22}$$

$$C_{FE} \approx \frac{1}{(\alpha_{01}+\alpha_{02})\left\{T - \dfrac{\alpha_{01}T_{01}+\alpha_{02}T_{02}}{(\alpha_{01}+\alpha_{02})}\right\}} \tag{23}$$

Hence equivalent anisotropy constant is $\alpha_{eq} = \alpha_{01} + \alpha_{02}$ and equivalent Curie Weiss temperature is $T_{C,eq} = \alpha_{01}T_1 + \alpha_{02}T_{02}/\alpha_{01} + \alpha_{02}$. Fig. 5(d) shows the simulated capacitance of isolated ferroelectric capacitor as a function of temperature. It can be clearly visualized that the as we increase the temperature the ferroelectric capacitance increases; this increase is only up to the curie temperature. Further if the temperature is increased, the capacitance starts decreasing. This trend is followed for all the three cases considered. Also, for the stacked ferroelectric case the curie temperature is in between the curie temperature of individual ferroelectric oxides. This is in line with the equation obtained in the above analysis. Fig. 5(e) depicts simulated capacitance of FE-FE-DE heterostructure as a function of temperature. It is interesting to note that when the dielectric is added in series to the isolated ferroelectric capacitor the curie temperature shift to lower value, this is for all the cases discussed. For $t_{FE2} = 0$, the new Curie Weiss temperature is $T_{01} - 1/\alpha_{01}C_{DE}$, while for $t_{FE1} = 0$, the new Curie Weiss temperature is $T_{02} - 1/\alpha_{02}C_{DE}$, and when $t_{FE2} = 108nm$ and $t_{FE1} = 120nm$ the new Curie Weiss temperature becomes $\alpha_{01}T_1 + \alpha_{02}T_{02}/\alpha_{01} + \alpha_{02} - 1/C_{DE}(\alpha_{01} + \alpha_{02})$. Fig. 5(f) depicts simulated amplification of FE-FE-DE heterostructure as a function of temperature which is obtained by solving the equation (24).

$$\frac{V_D}{V_S} = \frac{\dfrac{1}{(\alpha_{01}+\alpha_{02})\left\{T - \dfrac{\alpha_{01}T_{01}+\alpha_{02}T_{02}}{(\alpha_{01}+\alpha_{02})}\right\}}}{\dfrac{1}{(\alpha_{01}+\alpha_{02})\left\{T - \dfrac{\alpha_{01}T_{01}+\alpha_{02}T_{02}}{(\alpha_{01}+\alpha_{02})}\right\}} - C_{DE}} \tag{24}$$

Voltage amplification can be observed for all the three considered cases. Here it is interesting to note that the voltage amplification is highest when the temperature reaches its new curie Weiss temperature which was discussed earlier.

VII. CONCLUSION

We have explored the aspect of passive voltage amplification in FE-FE-DE heterostructure. It is observed that stacking of ferroelectric material, can lead cancellation of anisotropy constant (β), provided efficient tuning of ferroelectric thickness is done. This cancellation of the anisotropy constant is responsible for efficient capacitance matching between the ferroelectric and dielectric capacitance and hence forth voltage amplification in heterostructure. The findings show that the voltage amplification in stacked ferroelectric heterostructure is higher than the normal FE-DE heterostructure. Also, dynamic response and temperature analysis of FE-FE-DE heterostructure is studied further. It is observed that the curie temperature shifts to lower value when a dielectric capacitor is placed in series to the ferroelectric capacitor.

REFERENCES

[1] A. K. Bain and P. Chand, *Ferroelectrics: Principles and Applications*. Hoboken, NJ, USA: Wiley, 2017.

[2] Z. G. Ye, *Handbook of Dielectric, Piezoelectric and Ferroelectric Materials*. Cambridge, U.K.: Woodhead Publishing Materials Books, 2008, doi: 10.1201/9781439832882.

[3] B. Lang and H. L. W. Chan, *Frontiers of Ferroelectricity*. Boston, MA, USA: Springer, 2007, doi: 10.1007/978-0-387-38039-1.

[4] G. H. Haertling, "Ferroelectric ceramics: History and technology," *J. Amer. Ceram. Soc.*, vol. 82, no. 4, pp. 797–818, Apr. 1999, doi: 10.1111/j.1151-2916.1999.tb01840.x.

[5] P. Scherrer and G. Busch, "A century of ferroelectricity," *Nat. Mater.*, vol. 19, p. 129, 2020, doi: 10.1038/s41563-020-0611-1.

[6] W. Gao, Y. Zhu, Y. Wang, G. Yuan, and J.-M. Liu, "A review of flexible perovskite oxide ferroelectric films and their application," *J. Materiomics*, vol. 6, no. 1, pp. 1–16, Mar. 2020, doi: 10.1016/j.jmat.2019.11.001.

[7] Y. Xu, "3—Perovskite-type ferroelectrics: Part I," in *Ferroelectric Materials and their Applications*. Amsterdam, The Netherlands: Elsevier, 1991, pp. 101–162, doi: 10.1016/B978-0-444-88354-4.50008-5.

[8] Y. Xu, "4—Perovskite-type ferroelectrics: Part II," in *Ferroelectric Materials and Their Applications*. Amsterdam, The Netherlands: Elsevier, 1991, pp. 163–215, doi: 10.1016/B978-0-444-88354-4.50009-7.

[9] R. S. Roth, "Classification of perovskite and other ABO_3-type compounds," *J. Res. Nat. Bur. Standards*, vol. 58, no. 2, pp. 75–88, 1957.

[10] W. Cao, "Constructing Landau–Ginzburg–Devonshire type models for ferroelectric systems based on symmetry," *Ferroelectrics*, vol. 375, no. 1, pp. 28–39, 2008, doi: 10.1080/00150190802437845.

[11] A. I. Khan A., D. Bhowmik, P. Yu, S. J. Kim, X. Pan, R. Ramesh, and S. Salahuddin, "Experimental evidence of ferroelectric negative capacitance in nanoscale heterostructures," *Appl. Phys. Lett.*, vol. 99, Sep. 2011, Art. no. 113501, doi: 10.1063/1.3634072.

[12] M. Hoffmann, F. P. G. Fengler, M. Herzig, T. Mittmann, B. Max, U. Schroeder, R. Negrea, P. Lucian, S. Slesazeck, and T. Mikolajick, "Unveiling the double-well energy landscape in a ferroelectric layer," *Nature*, vol. 565, no. 7740, pp. 464–467 2019, doi: 10.1038/s41586-018-0854-z.

[13] A. K. Yadav, K. X. Nguyen, Z. Hong, P. García-Fernández, P. Aguado-Puente, C. T. Nelson, S. Das, B. Prasad, D. Kwon, S. Cheema, A. I. Khan, C. Hu, J. Ìñiguez, J. Junquera, L.-Q. Chen, D. A. Müller, R. Ramesh, and S. Salahuddin, "Spatially resolved steady-state negative capacitance," *Nature*, vol. 565, no. 7740, pp. 468–471, Jan. 2019, doi: 10.1038/s41586-018-0855-y.

[14] P. Zubko, J. C. Wojdel, M. Hadjimichael, S. Fernandez-Pena, A. Sené, I. Luk'yanchuk, J.-M. Triscone, and J. Ìñiguez, "Negative capacitance in multidomain ferroelectric superlattices," *Nature*, vol. 534, no. 7608, pp. 524–528, Jun. 2016, doi: 10.1038/nature17659.

[15] D. J. R. Appleby, N. K. Ponon, K. S. K. Kwa, B. Zou, P. K. Petrov, T. Wang, N. M. Alford, and A. O'Neill, "Experimental observation of negative capacitance in ferroelectrics at room temperature," *Nano Lett.*, vol. 14, no. 7, pp. 3864–3868, Jul. 2014, doi: 10.1021/nl5017255.

[16] V. V. Zhirnov and R. K. Cavin, "Negative capacitance to the rescue?" *Nature Nanotechnol.*, vol. 3, no. 2, pp. 77–78, Feb. 2008, doi: 10.1038/nnano.2008.18.

[17] M. H. Lee, K. T. Chen, C. Y. Liao, S. S. Gu, G. Y. Siang, Y. C. Chou, H. Y. Chen, J. Le, R.-C. Hong, Z. Y. Wang, and S. Y. Chen, "Extremely steep switch of negative-capacitance nanosheet GAA-FETs and FinFETs," in *IEDM Tech. Dig.*, San Francisco, CA, USA, 2018, p. 31, doi: 10.1109/IEDM.2018.8614510.

[18] W. Song, Y. Li, K. Zhang, X. Zou, J. Wang, Y. Kong, T. Chen, C. Jiang, C. Liu, L. Liao, and X. Liu, "Steep subthreshold swing in GaN negative capacitance field-effect transistors," *IEEE Trans. Electron Devices*, vol. 66, no. 10, pp. 4148–4150, Oct. 2019, doi: 10.1109/TED.2019.2934181.

[19] H. Amrouch, V. M. van Santen, G. Pahwa, Y. Chauhan, and J. Henkel, "NCFET to rescue technology scaling: Opportunities and challenges," in *Proc. 25th Asia South Pacific Design Automat. Conf. (ASP-DAC)*, Beijing, China, 2020, pp. 637–644, doi: 10.1109/ASP-DAC47756.2020.9045415.

[20] G. Paim, G. Zervakis, G. Pahwa, Y. S. Chauhan, E. A. C. da Costa, S. Bampi, J. Henkel, and H. Amrouch, "On the resiliency of NCFET circuits against voltage over-scaling," *IEEE Trans. Circuits Syst. I, Reg. Papers*, vol. 68, no. 4, pp. 1481–1492, Apr. 2021, doi: 10.1109/TCSI.2021.3058451.
[21] M. Yayla, K.-H. Chen, G. Zervakis, J. Henkel, J.-J. Chen, and H. Amrouch, "FeFET and NCFET for future neural networks: Visions and opportunities," in *Proc. Design, Automation Test Europe Conf. Exhib. (DATE)*, Grenoble, France, 2021, pp. 300–305, doi: 10.23919/DATE51398.2021.9473978.
[22] X. Li, J. Sampson, A. Khan, K. Ma, S. George, A. Aziz, S. K. Gupta, S. Salahuddin, M.-F. Chang, S. Datta, and V. Narayanan, "Enabling energy-efficient nonvolatile computing with negative capacitance FET," *IEEE Trans. Electron Devices*, vol. 64, no. 8, pp. 3452–3458, Aug. 2017, doi: 10.1109/TED.2017.2716338.
[23] K. M. Rabe, M. Dawber, C. Lichtensteiger, C. H. Ahn, and J.-M. Triscone, "Modern physics of ferroelectrics: Essential background," in *Physics of Ferroelectrics*. Berlin, Germany: Springer, 2007, pp. 1–30, doi: 10.1007/978-3-540-34591-6_1.
[24] H.-Z. Cao, Y.-G. Xiao, N.-J. Ma, L.-S. Yang, Y. Jiang, K. Xiong, G. Li, J. Ouyang, and M.-H. Tang, "Multiple factors of regulation for transient negative capacitance in $PbZr_{(1-x)}Ti_{(x)}O_3$ ferroelectric thin films," *Semicond. Sci. Technol.*, vol. 39, no. 2, Feb. 2024, Art. no. 025003, doi: 10.1088/1361-6641/ad1ba8.
[25] Y. Xiao, F. Tan, L. Yan, G. Li, M. Tang, and Z. Li, "Effect of depolarization field on steep switching characteristics in negative capacitance field effect transistors," *Semicond. Sci. Technol.*, vol. 35, no. 8, Aug. 2020, Art. no. 085005, doi: 10.1088/1361-6641/ab8d48.
[26] M. Budimir, D. Damjanovic, and N. Setter, "Piezoelectric response and free-energy instability in the perovskite crystals $BaTiO_3$, $PbTiO_3$, and $Pb(Zr,Ti)O_3$," *Phys. Rev. B, Condens. Matter*, vol. 73, no. 17, May 2006, Art. no. 174106, doi: 10.1103/physrevb.73.174106.
[27] B. Awadhiya, P. N. Kondekar, and A. D. Meshram, "Analogous behavior of FE-DE heterostructure at room temperature and ferroelectric capacitor at Curie temperature," *Superlattices Microstruct.*, vol. 123, pp. 306–310, Nov. 2018, doi: 10.1016/j.spmi.2018.09.015.
[28] Y. J. Kim, M. H. Park, Y. H. Lee, H. J. Kim, W. Jeon, T. Moon, K. Do Kim, D. S. Jeong, H. Yamada, and C. S. Hwang, "Frustration of negative capacitance in $Al_2O_3/BaTiO_3$ bilayer structure," *Sci. Rep.*, vol. 6, no. 1, p. 19039, Jan. 2016, doi: 10.1038/srep19039.
[29] B. Awadhiya, P. N. Kondekar, and A. D. Meshram, "Investigating undoped HfO_2 as ferroelectric oxide in leaky and non-leaky FE–DE heterostructure," *Trans. Electr. Electron. Mater.*, vol. 20, no. 5, pp. 467–472, Oct. 2019, doi: 10.1007/s42341-019-00137-3.
[30] B. Awadhiya, P. N. Kondekar, and A. D. Meshram, "Passive voltage amplification in non-leaky ferroelectric-dielectric heterostructure," *Micro Nano Lett.*, vol. 13, no. 10, pp. 1399–1403, Oct. 2018.
[31] G. Catalan, D. Jimenez, and A. Gruverman, "Negative capacitance detected," *Nat. Mater.*, vol. 14, no. 2, pp. 137–139, Jan. 2015, doi: 10.1038/nmat4195.
[32] A. I. Khan, K. Chatterjee, B. Wang, S. Drapcho, L. You, C. Serrao, S. R. Bakaul, R. Ramesh, and S. Salahuddin, "Negative capacitance in a ferroelectric capacitor," *Nature Mater.*, vol. 14, no. 2, pp. 182–186, Feb. 2015, doi: 10.1038/nmat4148.
[33] S. Salahuddin and S. Datta, "Use of negative capacitance to provide voltage amplification for low power nanoscale devices," *Nano Lett.*, vol. 8, no. 2, pp. 405–410, Feb. 2008, doi: 10.1021/nl071804g.
[34] A. I. Khan, "On the microscopic origin of negative capacitance in ferroelectric materials: A toy model," in *IEDM Tech. Dig.*, 2018, p. 9, doi: 10.1109/IEDM.2018.8614574.
[35] S. Yadav, P. Upadhyay, B. Awadhiya, and P. N. Kondekar, "Design and analysis of improved phase-transition FinFET utilizing negative capacitance," *IEEE Trans. Electron Devices*, vol. 68, no. 2, pp. 853–859, Feb. 2021, doi: 10.1109/TED.2020.3043222.
[36] S. Yadav, P. Upadhyay, B. Awadhiya, and P. N. Kondekar, "Ferroelectric negative-capacitance-assisted phase-transition field-effect transistor," *IEEE Trans. Ultrason., Ferroelectr., Freq. Control*, vol. 69, no. 2, pp. 863–869, Feb. 2022, doi: 10.1109/TUFFC.2021.3130194.
[37] R. K. Jaisawal, P. N. Kondekar, S. Yadav, P. Upadhyay, B. Awadhiya, and S. Rathore, "Insights into the operation of negative capacitance FinFET for low power logic applications," *Microelectron. J.*, vol. 119, Jan. 2022, Art. no. 105321, doi: 10.1016/j.mejo.2021.105321.
[38] B. Awadhiya, P. N. Kondekar, S. Yadav, and P. Upadhyay, "Insight into threshold voltage and drain induced barrier lowering in negative capacitance field effect transistor," *Trans. Electr. Electron. Mater.*, vol. 22, no. 3, pp. 267–273, Jun. 2021, doi: 10.1007/s42341-020-00230-y.
[39] S. Yadav, P. N. Kondekar, P. Upadhyay, and B. Awadhiya, "Negative capacitance based phase-transition FET for low power applications: Device-circuit co-design," *Microelectron. J.*, vol. 123, May 2022, Art. no. 105411, doi: 10.1016/j.mejo.2022.105411.
[40] B. Awadhiya, P. N. Kondekar, and A. D. Meshram, "Effect of ferroelectric thickness variation in undoped HfO_2-based negative-capacitance field-effect transistor," *J. Electron. Mater.*, vol. 48, no. 10, pp. 6762–6770, Aug. 2019, doi: 10.1007/s11664-019-07483-1.
[41] B. Awadhiya, P. N. Kondekar, and A. D. Meshram, "Understanding negative differential resistance and region of operation in undoped HfO_2-based negative capacitance field effect transistor," *Appl. Phys. A, Solids Surf.*, vol. 125, no. 6, Jun. 2019, pp. 1–7, doi: 10.1007/s00339-019-2718-2.
[42] B. Awadhiya, S. Yadav, P. Upadhyay, and P. N. Kondekar, "Effect of back gate biasing in negative capacitance field effect transistor," *Micro Nanostruct.*, vol. 166, Jun. 2022, Art. no. 207226, doi: 10.1016/j.micrna.2022.207226.
[43] S. Yadav, P. N. Kondekar, and B. Awadhiya, "Performance estimation of non-hysteretic negative capacitance FinFET based SRAM," *Microelectron. J.*, vol. 137, Jul. 2023, Art. no. 105796, doi: 10.1016/j.mejo.2023.105796.
[44] B. Awadhiya and S. Yadav, "Comparative study of negative capacitance field effect transistors with different doped hafnium oxides," *Microelectron. J.*, vol. 138, Aug. 2023, Art. no. 105838, doi: 10.1016/j.mejo.2023.105838.
[45] L. D. Landau and I. M. Khalatnikov, *On the Anomalous Absorption of Sound Near a Second Order Phase Transition Point* (Collected Papers), L. D. Landau, Ed. Amsterdam, The Netherlands: Elsevier, 1965, pp. 626–629, doi: 10.1016/B978-0-08-010586-4.50087-0.
[46] T. K. Song, "Landau–Khalatnikov simulations for ferroelectric switching in ferroelectric random access memory application," *J.-Korean Phys. Soc.*, vol. 46, no. 1, pp. 5–9, 2005.
[47] A. Jain and M. A. Alam, "Stability constraints define the minimum subthreshold swing of a negative capacitance field-effect transistor," *IEEE Trans. Electron Devices*, vol. 61, no. 7, pp. 2235–2242, Jul. 2014, doi: 10.1109/TED.2014.2316167.
[48] A. I. Khan, U. Radhakrishna, K. Chatterjee, S. Salahuddin, and D. A. Antoniadis, "Negative capacitance behavior in a leaky ferroelectric," *IEEE Trans. Electron Devices*, vol. 63, no. 11, pp. 4416–4422, Nov. 2016, doi: 10.1109/TED.2016.2612656.
[49] Y. G. Xiao, M. H. Tang, J. C. Li, P. C. Cheng, B. Jiang, H. Q. Cai, Z. H. Tang, X. S. Lv, and X. C. Gu, "Temperature effect on electrical characteristics of negative capacitance ferroelectric field-effect transistors," *Appl. Phys. Lett.*, vol. 100, no. 8, 2012, Art. no. 083508, doi: 10.1063/1.3688046.

BHASKAR AWADHIYA received the B.E. degree in electronics and communication engineering from Rajiv Gandhi Proudyogiki Vishwavidyalaya, Bhopal, India, in 2011, the M.Tech. degree in microelectronics from Manipal Institute of Technology, Manipal, India, in 2014, and the Ph.D. degree from the Pandit Dwarka Prasad Mishra Indian Institute of Information Technology, Design and Manufacturing, Jabalpur, India, in 2021. He is currently an Assistant Professor with the Department of Electronics and Communication Engineering, Manipal Institute of Technology, Manipal Academy of Higher Education, Manipal, Udupi, Karnataka, India. His current research interests include steep subthreshold slope (SS) devices and low-power devices.

SAMEER YADAV received the B.E. degree in electronics and communication engineering from Rajiv Gandhi Proudyogiki Vishwavidyalaya, Bhopal, India, in 2013, the M.Tech. degree in VLSI design from Indian Institute of Information and Technology, Gwalior, India, in 2016, and the Ph.D. degree in micro and nanoelectronics engineering from Indian Institute of Information and Technology, Jabalpur, India. He is currently an Assistant Professor with the Department of Electronics and Communication Engineering, Koneru Lakshmaiah Education Foundation, Vijayawada, Andhra Pradesh, India. His current research interests include device-circuit codesign, emerging low-power devices, and circuits for energy-efficient and high-performance computing.

YASHWANTH NANJAPPA (Senior Member, IEEE) received the B.E. degree in electronics and communication engineering from Visvesvaraya Technological University, Belagavi, in 2010, the M.Tech. degree in signal processing and VLSI from Jain University, Bengaluru, in 2012, and the Ph.D. degree from Visvesvaraya Technological University, in 2020. He is currently an Assistant Director (FDW) and an Assistant Professor—Senior Scale with the Department of Electronics and Communication Engineering, Manipal Institute of Technology, Manipal Academy of Higher Education, Manipal, actively undertaking numerous administrative and academic roles within the institute. His primary research interests include wireless sensor networks, communication systems, antennas, VLSI technology, and cyber security.

ABHISHEK PAHUJA received the B.E. and M.Tech. degrees from Rajiv Gandhi Proudyogiki Vishwavidyalaya, Bhopal, India, in 2009 and 2013, respectively, and the Ph.D. degree in electronics and communication engineering from the Pandit Dwarka Prasad Mishra Indian Institute of Information Technology, Design and Manufacturing Jabalpur (PDPM IIITDM Jabalpur), Jabalpur, India. He is currently an Associate Professor with the Department of Electronics and Communication Engineering, Koneru Lakshmaiah Education Foundation, Vijayawada, Andhra Pradesh, India. His current research interests include optoelectronics, plasmonics, photonics, energy harvesting for the IoT applications, and nanophotonics.

SHIVENDRA YADAV received the B.E. and M.Tech. degrees in electronics and communication engineering from Rajiv Gandhi Proudyogiki Vishwavidyalaya, Bhopal, India, in 2010 and 2015, respectively, and the Ph.D. degree in electronics and communication engineering from the Pandit Dwarka Prasad Mishra Indian Institute of Information Technology, Design and Manufacturing, Jabalpur, India, in 2020. He is currently an Assistant Professor with the Department of Electronics and Communication Engineering, Sardar Vallabhbhai National Institute of Technology, Surat, Gujrat, India. His research interests include the solar cells, simulation, and modeling of devices at nanoscale regimes, and memory designing.

SACHIN AGRAWAL received the M.E. degree from the Birla Institute of Technology Pilani, India, in 2009, and the Ph.D. degree from IIITDM Jabalpur, in 2018. Currently, he is an Assistant Professor with the National Institute of Technology Delhi. His research interests include RF energy harvesting, VLSI design, antenna designing, and mobile communication.